

1 **Supplementary information of “Significant production of ClNO₂ and possible source of**
2 **Cl₂ from N₂O₅ uptake at a rural site in eastern China”**

3 Men Xia^a, Xiang Peng^a, Weihao Wang^a, Chuan Yu^a, Peng Sun^b, Yuanyuan Li^b, Yuliang Liu^b,
4 Zhengning Xu^b, Zhe Wang^{a, c}, Zheng Xu^b, Wei Nie^b, Aijun Ding^b, and Tao Wang^{a, *}

5 ^aDepartment of Civil and Environmental Engineering, The Hong Kong Polytechnic University,
6 Hong Kong, China

7 ^b Joint International Research Laboratory of Atmospheric and Earth System Sciences, School
8 of Atmospheric Sciences, Nanjing University, Nanjing, 210023, China

9 ^c Now at Division of Environment and Sustainability, Hong Kong University of Science and
10 Technology, Hong Kong, China

11
12 * Correspondence to: Tao Wang (cetwang@polyu.edu.hk)

13
14 **Table of Contents**

15 **Text S1:** CIMS calibration and data validation

16 **S1.1.** Dependence of the N₂O₅ sensitivity on RH

17 **S1.2.** Isotopic analysis of ClNO₂ and Cl₂

18 **S1.3.** Potential interference from the inlet

19
20 **Table captions**

21 **Table S1.** Auxiliary measurements

22 **Table S2.** Summary of N₂O₅ uptake and ClNO₂ yield

23 **Table S3.** Uncertainty analysis of the measured and deducted parameters

24
25 **Figure captions**

26 **Figure S1.** Comparison of O₃ at the SORPES site and the SAS site

27 **Figure S2.** Isotopic analysis of ClNO₂ and Cl₂

28 **Figure S3.** Dependence of the N₂O₅ sensitivity on RH

29 **Figure S4.** Comparison of ACSM and MARGA data

30 **Figure S5.** An example showing the calculation of $\gamma(\text{N}_2\text{O}_5)$ and $\phi(\text{ClNO}_2)$

31 **Figure S6.** Dependence of $\gamma(\text{N}_2\text{O}_5)$ on [H₂O]

32 **Figure S7.** Investigation of the potential of sulfate and total aerosol organics to consume NO₂⁺

33
34 **References**

35
36 **Text S1:** CIMS calibrations and data validation

37 **S1.1.** Dependence of the N₂O₅ sensitivity on RH

38 In the ion molecular reaction (IMR) chamber, the reagent ion I⁻ reacts with H₂O to form the
39 iodide water cluster, I(H₂O) which also reacts with N₂O₅ to produce IN₂O₅⁻ (Kercher et al.,
40 2009). Also, N₂O₅ may undergo hydrolysis in the sampling system. Thus, the sensitivity of N₂O₅
41 depends on the RH. In this study, the N₂O₅ signal was normalized to the I(H₂O)⁻ signal (Hz 145)
42 to account for the change of primary ions. During the field measurements, we monitored the
43 RH at the indoor inlet of CIMS. When conducting calibrations, we tested the relationship
44 between the normalized N₂O₅ sensitivity and RH (Fig. S3). A quadratic relationship in Fig. S3
45 ($y = -3.78 \times 10^{-9}x^2 + 1.69 \times 10^{-7}x + 1.72 \times 10^{-5}$) was used to correct the RH effect on the ambient N₂O₅
46 data.

47

48 **S1.2. Isotopic analysis of ClNO₂ and Cl₂**

49 The ClNO₂ signals were recorded at mass 208 and 210 amu, representing ³⁵ClNO₂ and
50 ³⁷ClNO₂, respectively. The relationship between the 208 signals and the 210 signals was
51 examined (Fig. S2). During ambient samplings, the slope of the Hz 210-Hz 208 plot was 0.3135
52 with R²=0.998 (Fig. S2a). And the slope was 0.3154 with R²=0.999 (Fig. S2a) during
53 calibrations. The isotopic analysis was also performed for Cl₂. The correlations between mass
54 197 amu (³⁵Cl³⁵Cl) and 199 amu (³⁵Cl³⁷Cl) were excellent with R²=0.999 for calibration data
55 and R²=0.965 for the ambient data (Fig. S2b). The slope of the plot was 0.599 and 0.558 for the
56 ambient data and calibration data, respectively, which is similar to previous studies (Liao et al.,
57 2014). These results confirmed the identity of ClNO₂ and Cl₂ and indicated virtually no
58 interference for ClNO₂ and negligible interference for Cl₂.

59

60 **S1.3 Potential artifact of the inlet**

61 When sampling ambient air, ambient particles gradually deposit on the inner wall of the
62 sampling tubing. After a period of time, N₂O₅ in the ambient air reacts with the deposited
63 particles, resulting in N₂O₅ loss and ClNO₂ formation. This inlet chemistry may cause
64 underestimation of N₂O₅ and overestimation of ClNO₂. To minimize the interference from the
65 sampling inlet, we adopted a virtual impactor design and a by-pass flow. The inlet design
66 ensured that larger particles were mostly pumped through the by-pass flow. And the increased
67 total flow (10 Lpm) reduced the residence time of N₂O₅ on the inlet. The sampling line was
68 replaced daily by a cleansed one just before dusk to achieve minimum artifact on nighttime
69 measurements.

70 We quantified the percentage of N₂O₅ loss and ClNO₂ formation in the inlet under different

71 RH. After sampling for 24 hours, the used sampling line was taken indoor and connected to a
 72 zero-air generator with a flow rate of 10 Lpm. Then, we injected N_2O_5 at one end of the
 73 sampling line and measured the outflow at the other end in CIMS. The injected mixing ratios
 74 of N_2O_5 was determined by introducing N_2O_5 directly into the CIMS without passing the
 75 sampling line. The CIMS only inhaled ~ 1.5 Lpm airflow while the remaining ~ 8.5 Lpm airflow
 76 was discarded as a by-pass flow. The percentage of N_2O_5 loss and $ClNO_2$ yield ($ClNO_2$
 77 production divided by N_2O_5 loss) increased with RH. When RH = 40 %, the N_2O_5 loss was
 78 16.6 %. Thus, we assumed that the inlet artifact caused up to 16.6 % uncertainties for the
 79 ambient measurement of N_2O_5 and $ClNO_2$. 40 % RH was selected because the average RH
 80 recorded at the inlet of the CIMS was 40 % during the whole campaign. Cl_2 formation on the
 81 sampling tube was negligible in the wall-loss testing.

82

83

84 **Table S1.** Measuring technique, detection limit and time resolution of the instruments in the
 85 field study. Detection limits were determined by 3σ of the noise level in 10 min.

Measured species	Techniques	Detection limits	Time resolution
N_2O_5 , $ClNO_2$, Cl_2 , $HOCl$, $BrCl$	Q-CIMS	5~8 pptv	10 s
NO , NO_2	Chemiluminescence with photolytical converter	0.06 ppbv	1 min
NO_y	Chemiluminescence with MoO converter	0.1 ppbv	1 min
CO	Infrared photometry	4 ppbv	1 min
SO_2	Pulsed ultraviolet fluorescence	0.1 ppbv	1 min
O_3	Ultraviolet photometry	0.5 ppbv	1 min
$HONO$	LOPAP	5 pptv	1 min
HNO_3	ion chromatography	0.05 ppbv	1 hour
$PM_{2.5}$	TEOM	$1 \mu g/m^3$	1 min
NH_4^+ , Cl^- , NO_3^- , SO_4^{2-}	ToF-ACSM	$0.01\sim 0.06 \mu g/m^3$	10 min
jNO_2	Filter radiometer	$4 \times 10^{-5} s^{-1}$	10 s
VOCs	PTR-TOF-MS	10 pptv	10 min

86

87 **Table S2.** Summary of $\gamma(N_2O_5)$, $\phi(ClNO_2)$, and $\phi(Cl_2)$ (where applicable) in the selected 15
 88 nighttime cases.

plume	start	end	$\gamma(N_2O_5)$	$\phi(ClNO_2)$	$\phi(Cl_2)$
1	4/12/18 2:10	4/12/18 3:00	0.0043	0.885	0.037 ± 0.004
2	4/12/18 3:10	4/12/18 3:40	0.0068	0.716	0.021 ± 0.003
3	4/12/18 21:40	4/13/18 0:40	0.0061	0.853	0.036 ± 0.004
4	4/16/18 19:50	4/16/18 20:30	0.0031	0.378	0.013 ± 0.000

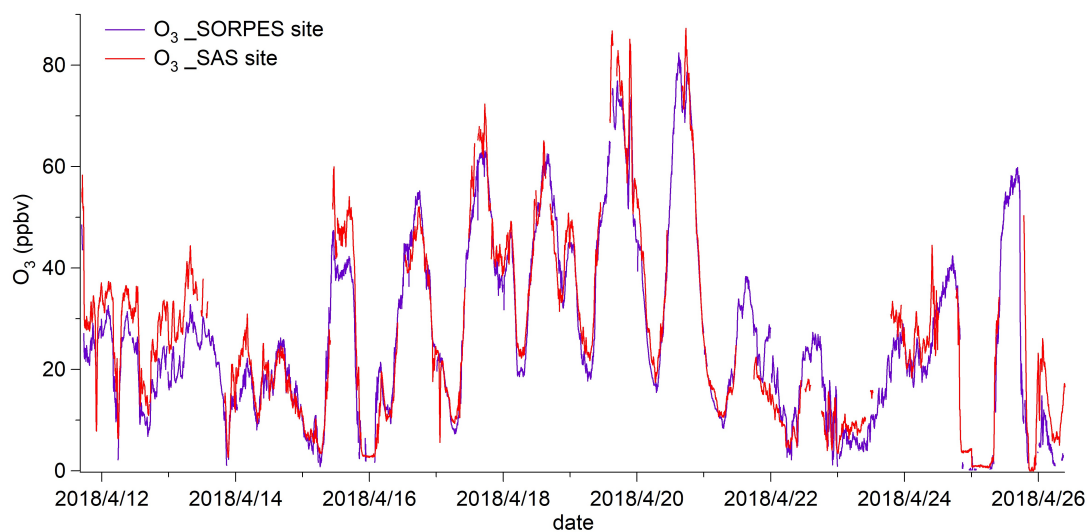
5	4/16/18 20:40	4/16/18 21:20	0.0033	0.541	0.012±0.001
6	4/17/18 22:20	4/17/18 23:40	0.0058	0.521	0.010±0.001
7	4/18/18 3:00	4/18/18 3:50	0.0135	0.483	-
8	4/18/18 4:10	4/18/18 4:40	0.0139	0.187	-
9	4/19/18 0:00	4/19/18 0:40	0.0055	0.280	0.014±0.001
10	4/19/18 0:40	4/19/18 1:40	0.0041	0.523	0.018±0.002
11	4/19/18 2:00	4/19/18 3:00	0.0091	0.769	0.006±0.001
12	4/20/18 1:00	4/20/18 2:00	0.0084	0.641	0.013±0.001
13	4/20/18 2:10	4/20/18 2:50	0.0074	0.647	0.013±0.000
14	4/26/18 1:20	4/26/18 2:00	0.0136	0.468	0.006±0.001
15	4/26/18 2:30	4/26/18 3:20	0.0125	0.533	0.013±0.002
Average ± standard deviation			0.008±0.004	0.562±0.197	0.016±0.010

89

90 **Table S3.** Uncertainty analysis of the measured and deduced parameters. The uncertainty of
91 Cl⁻, NO₃⁻, SO₄²⁻, and S_a were referred to previous studies (Tham et al., 2016;Tham et al., 2018).

Parameter	sources of uncertainty (if any)			Propagated error	Reference
N ₂ O ₅ , ClNO ₂	Signal precision	calibration	inlet interference	18.8 %	This study
	3.0 %	8.3 %	16.6 %		
Cl ₂	Signal precision	calibration	inlet interference	10.4 %	This study
	3.0 %	10.0 %	neglected		
[Cl ⁻], [NO ₃ ⁻], [H ₂ O]	ACSM		E-AIM model	18.0 %	This study
	10.0 %		15 % (assumed)		
[H ⁺]	Cl ⁻ , NO ₃ ⁻ , SO ₄ ²⁻ , NH ₄ ⁺		E-AIM model	25.0 %	This study
	10 %, 10 %, 10 %, 10 %		15 % (assumed)		
γ(N ₂ O ₅)	N ₂ O ₅ , ClNO ₂	NO ₃ ⁻	S _a	34.2 %	This study
	18.8 %, 18.8 %	10.0 %	19.0 %		
φ(ClNO ₂)	ClNO ₂	NO ₃ ⁻		21.3 %	This study
	18.8 %	10.0 %			
φ(Cl ₂)	γ(N ₂ O ₅)	N ₂ O ₅ , Cl ₂	S _a	44.6 %	This study
	34.2 %	18.8 %, 10.4 %	19.0 %		
Cl ⁻ , NO ₃ ⁻ , H ₂ O				10.0 %	Tham et al. 2016
S _a				19.0 %	Tham et al. 2018

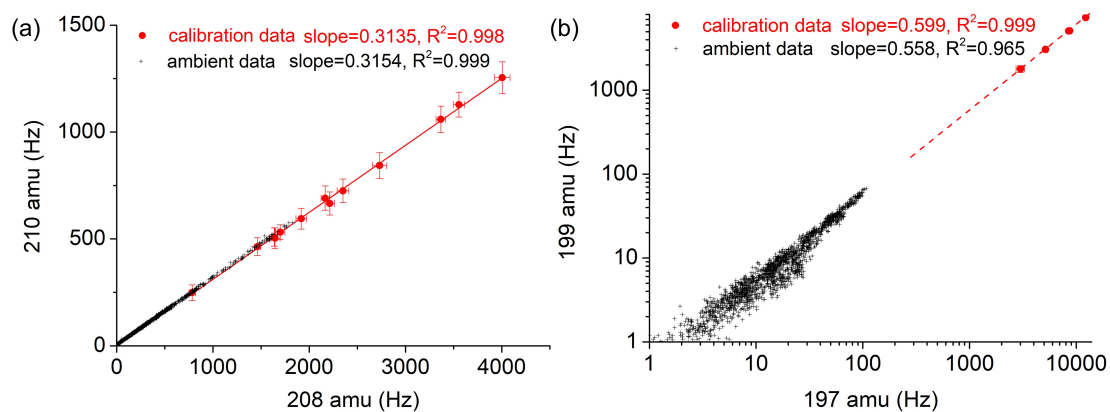
92



93

94 **Figure S1.** Comparison of O₃ measurements at the SORPES site and the SAS site.

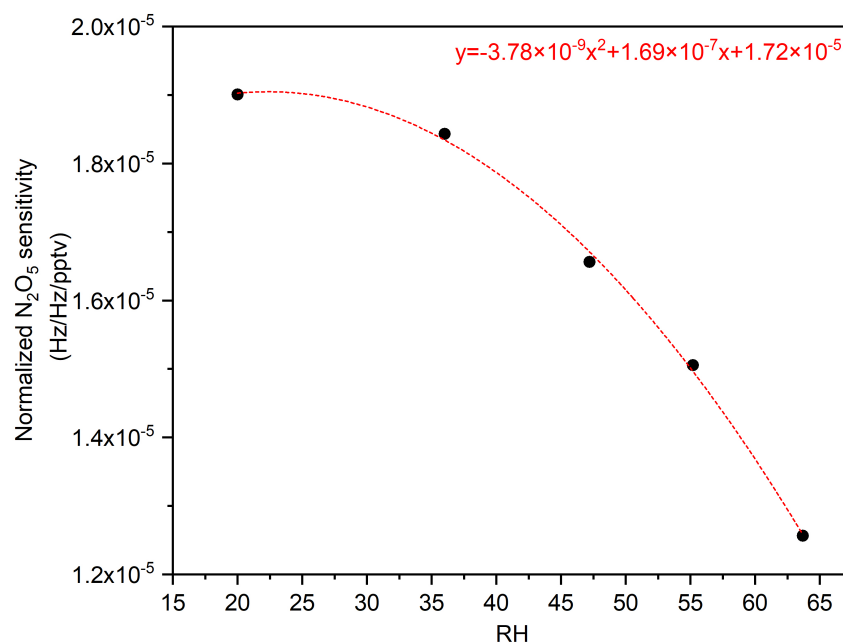
95



96

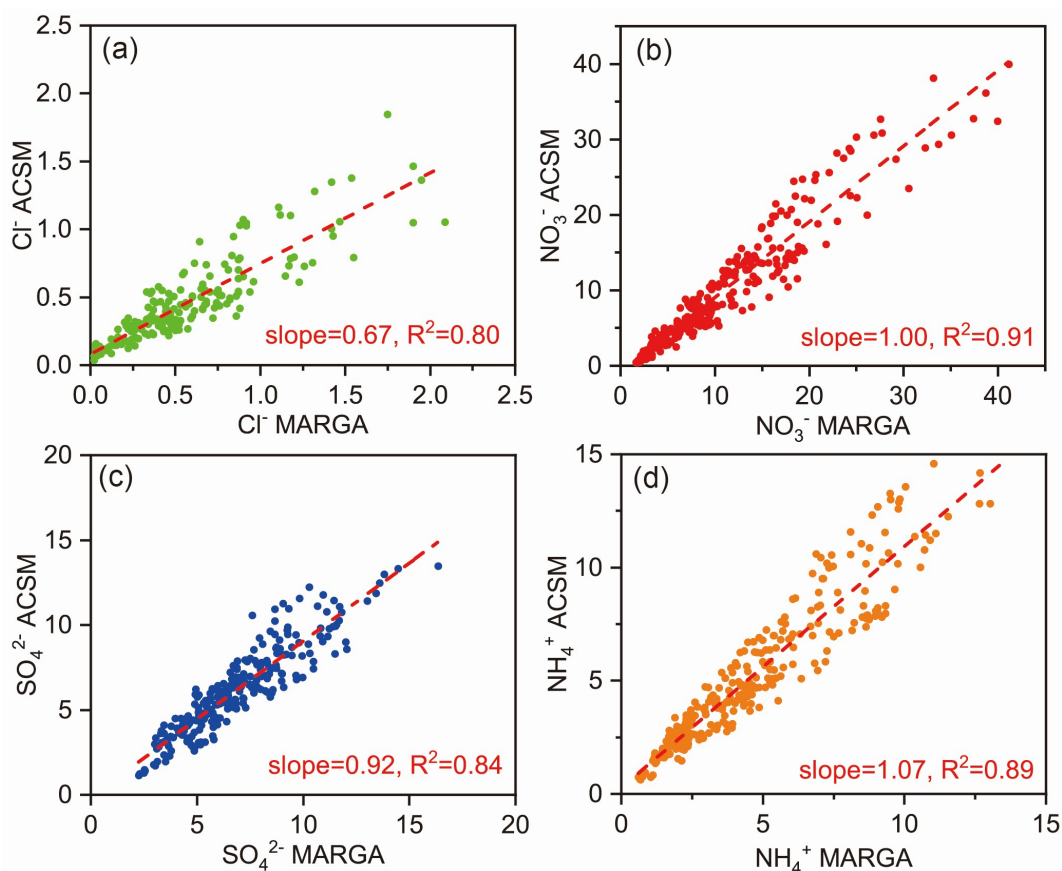
97 **Figure S2 .** Isotopic analysis of (a) ClNO₂ and (b) Cl₂. The red dots and corresponding fitting
 98 lines represent calibration data, while the black crosses “+” denote ambient data.

99

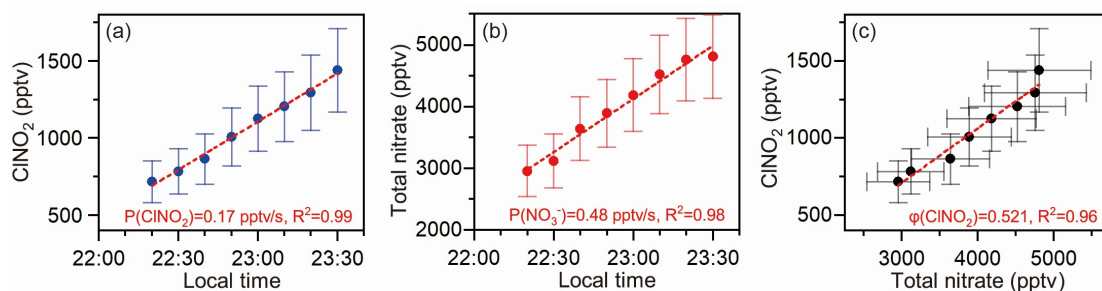


100

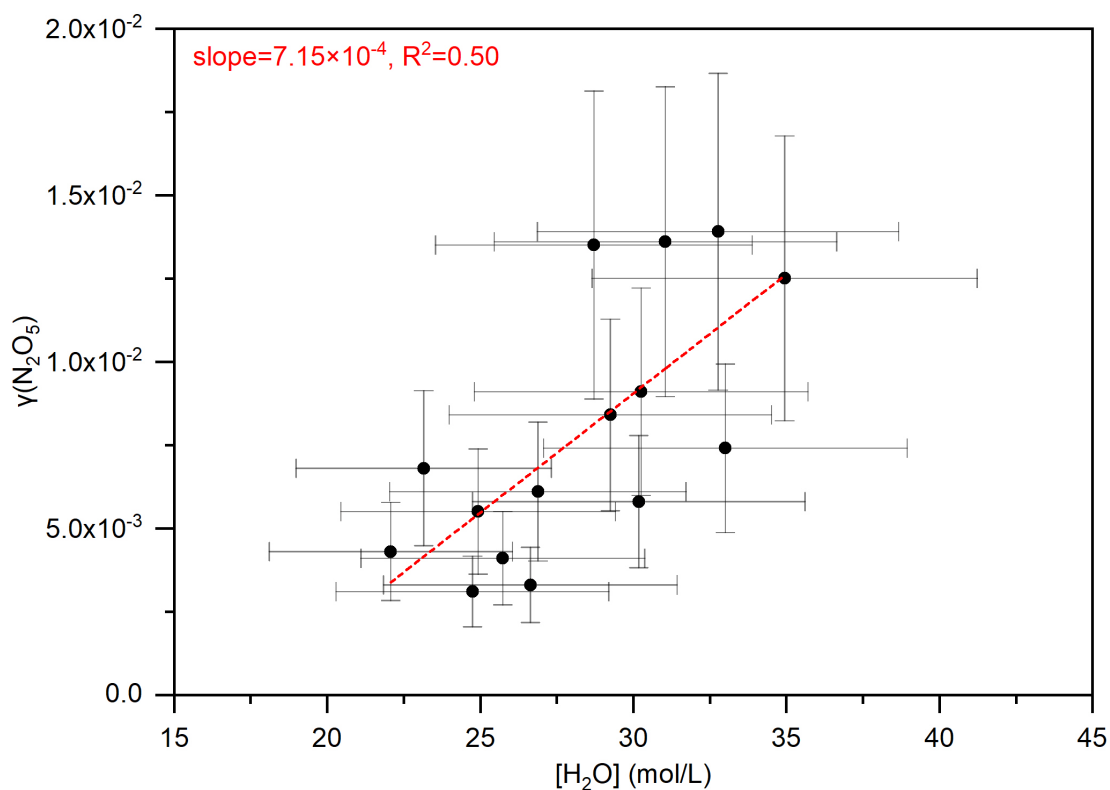
101 **Figure S3.** Dependence of the N_2O_5 sensitivity on RH. The normalized sensitivity of N_2O_5 (y
 102 axis) was fitted as a quadratic function of RH (x axis), which is $y = -3.78 \times 10^{-9}x^2 + 1.69 \times 10^{-7}x + 1.72 \times 10^{-5}$ ($R^2=1$).
 103
 104



105 **Figure S4.** Comparison of ACSM and MARGA data. (a), (b), (c), and (d) showed the
 106 comparison of Cl^- , NO_3^- , SO_4^{2-} , and NH_4^+ during the whole campaign, respectively. Since the
 107 resolution of the MARGA data was 1 hour, the ACSM data was averaged to 1 hour. Units of
 108 the ions are all $\mu\text{g}/\text{m}^3$.
 109
 110

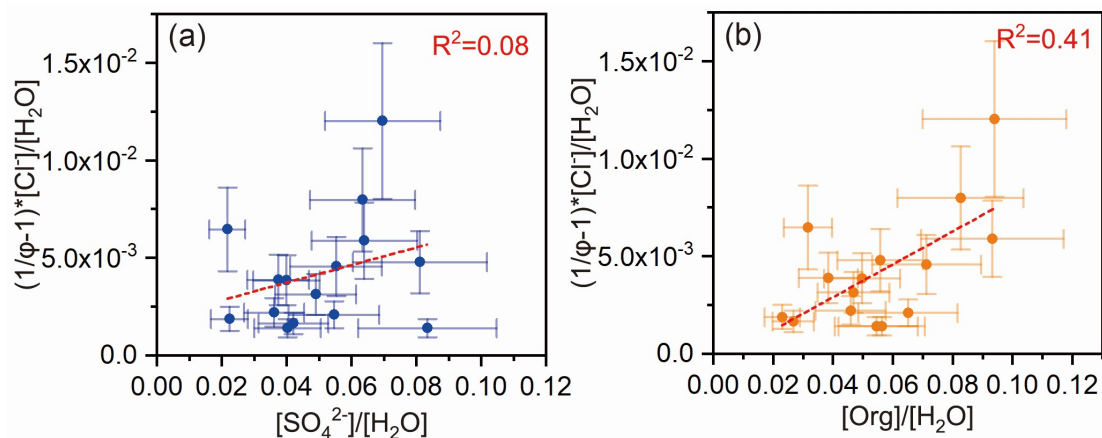


111 **Figure S5.** An example showing the calculation of $\gamma(\text{N}_2\text{O}_5)$ and $\phi(\text{ClNO}_2)$. (a) and (b) show
 112 the increasing rate of ClNO_2 and total nitrate observed on the night of Apr 17. (c) displays the
 113 relationship between ClNO_2 and total nitrate shown in (a) and (b).
 114
 115



116
117
118

Figure S6. Dependence of $\gamma(\text{N}_2\text{O}_5)$ on $[\text{H}_2\text{O}]$.



119
120
121
122

Figure S7. Investigation of the potential of sulfate and total aerosol organics to consume NO_2^+ .
(a) and (b) represent sulfate and total organic aerosols, respectively.

123

References

124 Kercher, J., Riedel, T., and Thornton, J.: Chlorine activation by N_2O_5 : simultaneous, in situ
125 detection of ClNO_2 and N_2O_5 by chemical ionization mass spectrometry, Atmospheric
126 Measurement Techniques, 2, 193-204, 2009.
127 Liao, J., Huey, L. G., Liu, Z., Tanner, D. J., Cantrell, C. A., Orlando, J. J., Flocke, F. M., Shepson,
128 P. B., Weinheimer, A. J., and Hall, S. R.: High levels of molecular chlorine in the Arctic
129 atmosphere, Nature Geoscience, 7, 91, 2014.
130 Tham, Y. J., Wang, Z., Li, Q., Yun, H., Wang, W., Wang, X., Xue, L., Lu, K., Ma, N., Bohn, B.,
131 Li, X., Kecorius, S., Groß, J., Shao, M., Wiedensohler, A., Zhang, Y., and Wang, T.: Significant

132 concentrations of nitryl chloride sustained in the morning: investigations of the causes and
133 impacts on ozone production in a polluted region of northern China, *Atmospheric Chemistry
134 and Physics*, 16, 14959-14977, 10.5194/acp-16-14959-2016, 2016.
135 Tham, Y. J., Wang, Z., Li, Q., Wang, W., Wang, X., Lu, K., Ma, N., Yan, C., Kecorius, S., and
136 Wiedensohler, A.: Heterogeneous N₂O₅ uptake coefficient and production yield of ClNO₂ in
137 polluted northern China: Roles of aerosol water content and chemical composition, 2018.
138